Engineering Structures 189 (2019) 423–439

Contents lists available at ScienceDirect

Engineering Structures

journal homepage: www.elsevier.com/locate/engstruct

Cyclic behavior of reinforced concrete cladding panels connected with energy dissipative steel cushions

Faruk Karadoğan[a], Ercan Yüksel[b,*], Arastoo Khajehdehi[c], Hasan Özkaynak[d], Ahmet Güllü[e], Erkan Şenol[c]

[a] Isik University, Department of Civil Engineering, Sile, Istanbul, Turkey
[b] Istanbul Technical University, Faculty of Civil Engineering, Maslak, Istanbul, Turkey
[c] Istanbul Technical University, Institute for Science and Technology, Maslak, Istanbul, Turkey
[d] Beykent University, Department of Civil Engineering, Maslak, Istanbul, Turkey
[e] Istanbul Gedik University, Department of Civil Engineering, Kartal, Istanbul, Turkey

ARTICLE INFO

Keywords:
Cladding panel
Connection device
Energy dissipation
Steel cushion

ABSTRACT

Precast concrete structures show damage after the destructive earthquakes and indicate that the connections of reinforced concrete (RC) cladding panels might be inadequate. RC cladding panels greatly increase the lateral stiffness and strength of the building when they are rigidly connected to the structural system. However, this also increases the seismic requirements. Consequently, a robust mechanical connection device with energy-dissipating capability was produced for RC cladding panels. Extensive experimental and numerical studies on an energy-dissipative steel cushion (SC) connection device were carried out in the framework of the SAFECLADDING project. Cladding panel tests were conducted with various connection configurations. The fundamental variables are the location, quantity, and thickness of SCs used in the cladding systems. The test results demonstrate that the SCs used in panel-to-panel and panel-to-support connections made large contributions to the total energy dissipation capacity. The parameters of a numerical model were also evaluated to reproduce the experimental results.

1. Introduction

Reinforced concrete (RC) panels are used in cladding systems in the façades of precast structures to provide thermal insulation, weather resistance, and improved building appearance. They are commonly evaluated as non-structural elements. Different connection forms could be applied for the connections of RC cladding panels, free-to-slide, free-to-rotate, and fixed connections. The collapse of cladding panels is common due to connection failures from seismic damage in industrial RC precast structures, as reported by Ercolino et al. [1]. The damage is related to the interaction between the panels and the main structure. They performed nonlinear time history analyses on several models by considering the panel-to-structure interaction and roof diaphragm. High forces at the panel-to-structure connection were computed by numerical analyses and verified the early collapse of these connections due to seismic actions. The requirements were found to be much larger than the shear capacity of the connection.

Priestley et al. [2] performed studies on precast concrete walls with self-centering components in the Precast Seismic Structural Systems (PRESSS) research program. They tested an unbounded post-tensioned precast wall system consisting of two walls and connectors that resist lateral forces in one direction. The connectors performed well, and no structural damage was observed. Psycharis et al. [3] performed experimental and numerical investigations on the monotonic and cyclic behavior of integrated connections of cladding panels. The experimental results showed that integrated connections have considerable ductility capacity. However, significant openings were also observed at the joints.

Biondini et al. [4] investigated the seismic behavior of a precast structural frame with a new type of connection system for cladding panels. The results of nonlinear dynamic analyses highlighted the role of panel connections on the seismic behavior and showed the effectiveness of the dual frame/wall system with dissipative connections. Dal Lago et al. [5] proposed friction-based and plasticity-based energy dissipative connector devices for the seismic design of precast structures with cladding panels. These connectors were used to join two adjacent panels or one panel to surrounding structural components to limit displacement demands and control the seismic forces. The

* Corresponding author.
E-mail address: yukselerc@itu.edu.tr (E. Yüksel).

https://doi.org/10.1016/j.engstruct.2019.03.092
Received 19 July 2018; Received in revised form 25 March 2019; Accepted 25 March 2019
Available online 01 April 2019

Table 1
Definition of the specimens.

Test #	Designation	Connection		
		PB t_1 (mm)	PP t_2 (mm)	PS t_3 (mm)
I	S-PB3.PP5.PS8	3	5	8
II	D-PB3.PP5.PS8	3	5	8
III	D-PB5.PP5.PS8	5	5	8
IV	S-PB8.PP5.PS8	8	5	8
V	S-PB8.PP8.PS8	8	8	8
VI	D-PB8.PS3	8	N/A	3
VII	D-PB8.PP5.PS3	8	5	3
VIII	D-PB8.PP8.PS3	8	8	3
IX	D-PB8.PP5.PS5	8	5	5
X	D-PB8.PP3.PS5	8	3	5

S: Single SC at the base level, D: Double SCs at the base level.

efficiency of the proposed connectors was demonstrated through monotonic and cyclic experiments and numerical investigations in the framework of the SAFECLADDING project. The results showed the effectiveness of the proposed connectors in improving the seismic response of precast structures by means of restriction in force and displacement demands. In addition, design guidelines for each type of connectors and equipped structural systems were provided.

Dal Lago and Tornaghi [6] conducted experimental studies on innovative panel-to-structure sliding connectors to determine their behavior under imposed displacement histories with the application of constant normal force. The static and dynamic friction coefficients were derived from the experiments. They also provided design rules for the assessment of the seismic performance of panels equipped with this type of sliding connector based on the evaluated friction coefficients. The connector can isolate the in-plane motion of cladding panels from the structure to preclude failure due to coupling of the cladding panels and frame during seismic excitations.

Dal Lago et al. [7] carried out experiments on single connectors and structural subassemblies of full-scale panels. The connectors exhibited a quasi-rigid pseudo-plastic behavior in the experiments with a typical friction-type cyclic behavior and large energy-dissipation capacity. The cyclic stability of connectors with brass sheets could allow them to be re-used after large amplitude cycles. Experiments were performed on a full-scale precast structure and showed that the proposed connectors can increase the structural damping properties and reduce structural drifts with controlled forces.

Del Monte et al. [8] presented the results of an experimental study on both commercial and innovative mechanical cladding-to-structure connections. The observed damage modes for the commercial mechanical connecters included flexural failure of the strap, failure of the anchor channel fixed to beams or columns, and removal of the hammer-head screws. The innovative connections demonstrated that the in-plane horizontal displacement of panels and the structure can be detached.

Ductile mechanical devices are promising for robust connections of RC panels. There are innovative efforts to generate seismic energy dissipation in the connections of RC cladding panels to reduce the structural damages in the main structure. Dal Lago et al. [9] presented a study about the seismic performance of precast frame-type structures based on the behavior of mechanical connector devices used for both structural and non-structural components. A design solution involving a controlled RC cladding-structure was proposed using the results of linear and nonlinear time history analyses. It was concluded that the forces in the RC panel on the main structure connections might be limited with dissipative cladding connection systems. Furthermore, using low-cost dissipative devices between the cladding panels and between the roof elements could significantly improve the seismic performance.

Kelly et al. [10] conducted Pioneering studies about energy-dissipating connection devices to determine the energy absorption capacity of flat U strips. They concluded that U strips have quite high energy dissipation capacity. Oh et al. [11] performed cyclic tests on full-scale specimens instrumented with slit dampers at beam-to-column connections. The test results showed that plastic deformations in the system were concentrated at only the dampers and connections.

Shultz and Magana [12] conducted an experimental study on the behavior of different shear connectors. They investigated the performance of U-shaped flexure plate (UFP) connectors, which were used as horizontal and vertical joint connectors in a PRESSS test building. The UFP connector was proposed as an energy-dissipating flexible connector. As a real application, U UFP dissipaters were installed in a hospital building in New Zealand, which had been completed one month before the largest earthquake. The building suffered minor damage to non-structural components, with some damage to services requiring repair.

Chan and Albermani [13] performed studies on a new steel energy-dissipative device called a steel slit damper, which was designed for the protection of structures against earthquakes. It was fabricated from a standard structural wide-flange section with a number of slits cut from the web. The device exhibited stable hysteresis in the experiments with excellent energy dissipation and ductility. Biondini et al. [14] conducted monotonic and cyclic experiments on single connectors and two full-scale structural sub-assemblies. The connection system consisted of friction-based or plasticity-based devices located in the joints of vertical and horizontal panels. Tests were performed on both the friction-based and plasticity-based devices and highlighted their good hysteretic behavior and energy dissipation capacity. Numerical studies showed remarkable seismic improvement of precast structures with dissipative connections. Moreover, the devices were able to limit the forces and displacements.

Yüksel et al. [15] performed experimental and numerical studies on SCs subjected to combined actions of shear and normal forces. Closed-form equations were derived to predict global response of SCs. High energy dissipation capacity and high ductile behavior were obtained under bi-directional loading. Özkaynak et al. [16] investigated the cyclic behavior of SCs under uniaxial shear and normal forces. The results showed that SCs have large deformation and high energy dissipation capacities, as well as stable response behavior under uniaxial effects.

Özkaynak et al. [17] carried out experiments to identify the effects of material quality and the welding location on the cyclic behavior of SCs. The stainless steel specimens had lower strength and energy-dissipation capacity than ones made from mild steel. The best performance was obtained with the specimens in which the welding positioned was

Table 2
Definition of the tests.

Test variable	Target of the investigation	Tests #
Number of SCs in PS connection	The effect of number of SCs used in PS connection	I, II
SC thickness in PB connection	The effect of SC thickness used in PB connection for the specimens supported by double SCs	II, III
SC thickness in PP connection	The effect of SC thickness used in PP connection for the specimens supported by single SC	IV, V
	The effect of SC thickness used in PP connection for the specimens supported by double SC	VI, VII, VIII and IX, X
SC thickness in PS connection	The effect of SC thickness used in PS connection	VII, IX

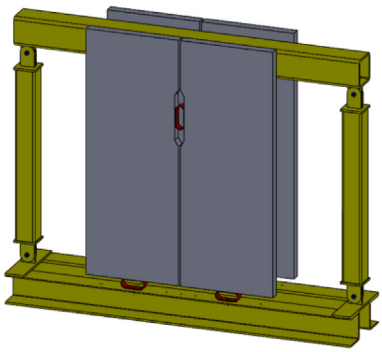

(a) 3D view of the specimen with single SC at PS connection

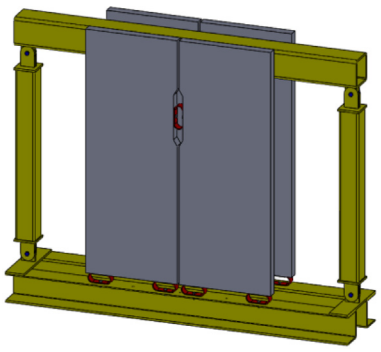

(b) 3D view of the specimen with double SCs at PS connection

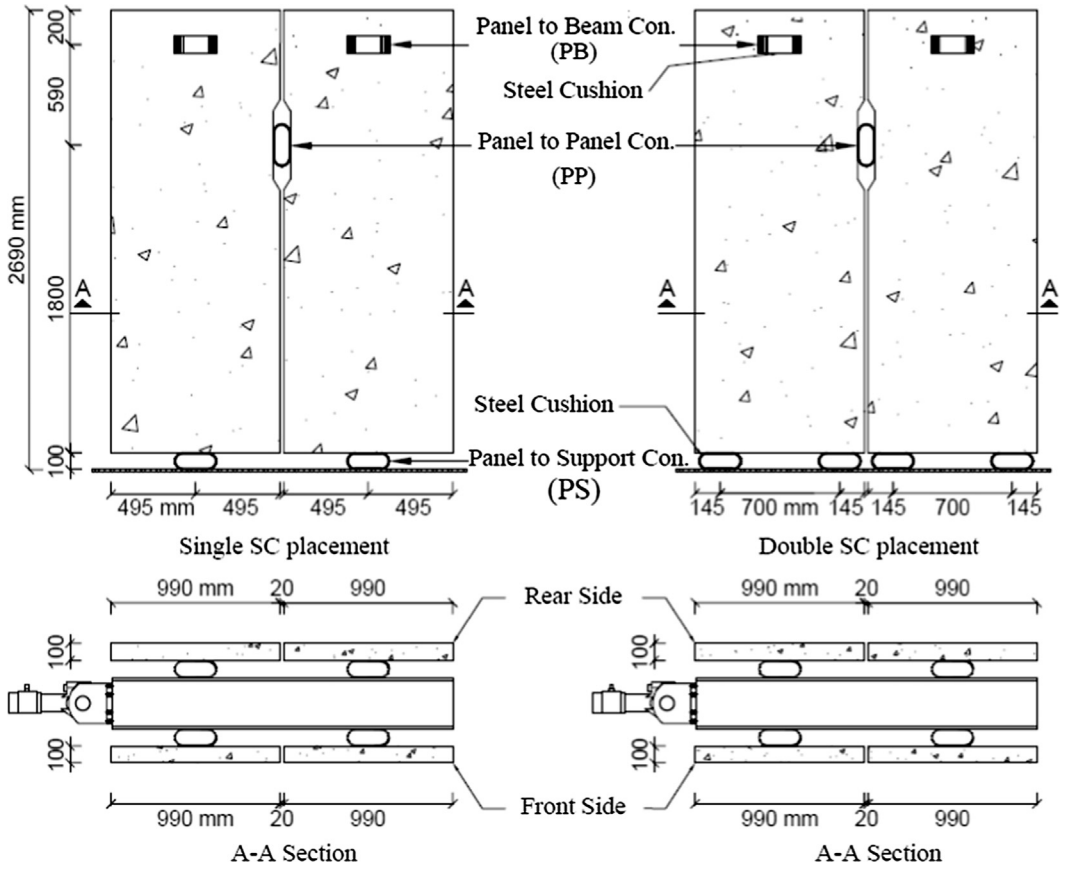

(c) Dimensions of the specimens and placement of SCs

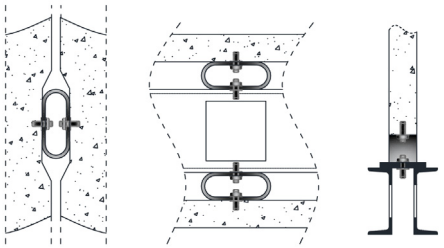

(d) The connection details of SCs

Fig. 1. Test setup and properties of the specimens.

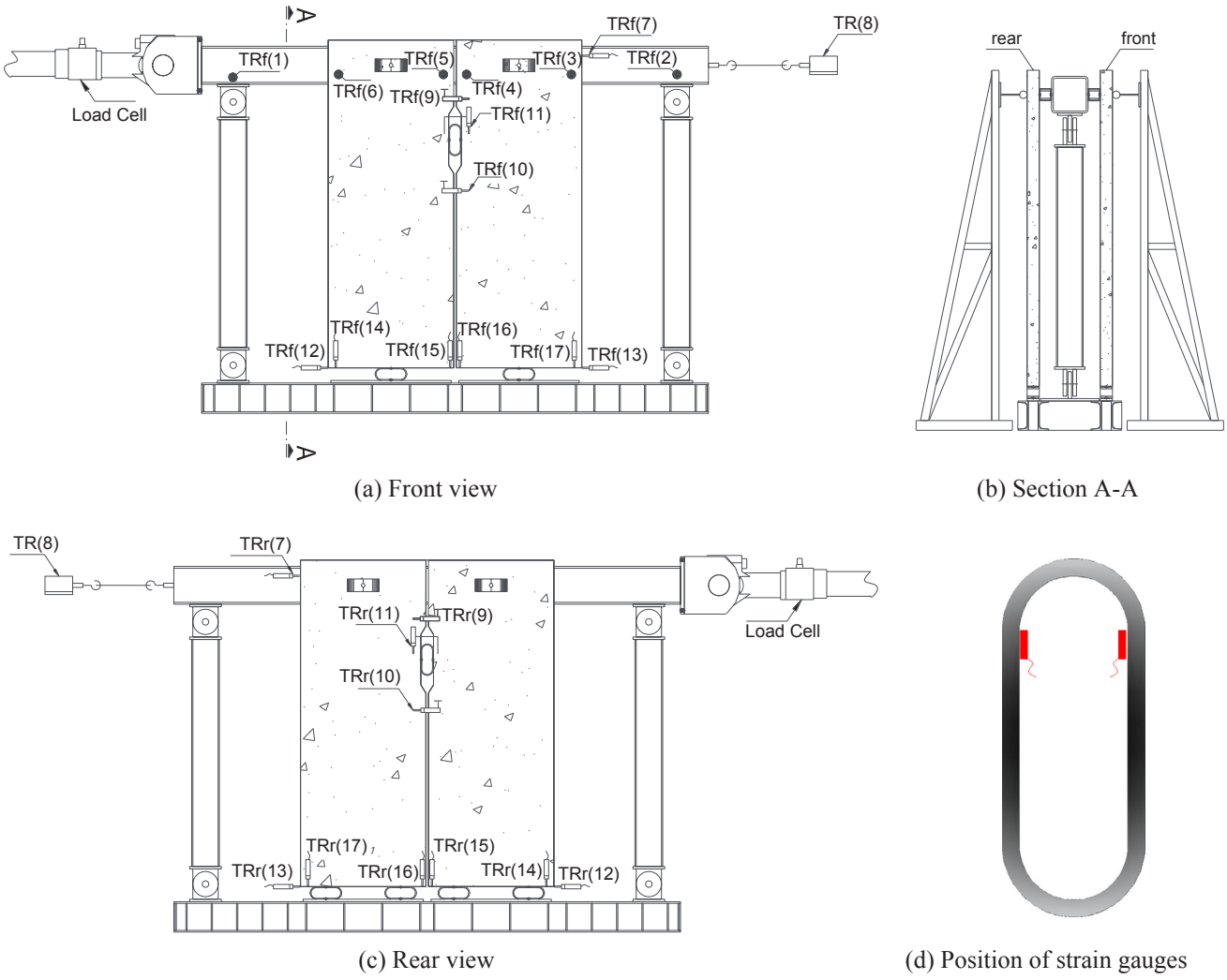

Fig. 2. Placements of displacement transducers and strain gauges.

at the mid-height of the SC. Özkaynak et al. [18] performed some tests to determine the behavior of SCs under variable axial loading. The normal force polarity and intensity were particularly influential on the behavior.

The motivation of this study is to use SCs as robust mechanical devices with energy-dissipating capability for the connections of RC cladding panels. The efficiency of the connection technique was evaluated under in-plane lateral loads through laboratory tests. Numerical models are also presented to reproduce the experimental results.

2. Experimental study

2.1. Specimens and test setup

The dimensions of the tested RC panels were selected as 990 mm × 2690 mm × 100 mm by accounting for laboratory restrictions. A special testing setup was used to generate displacement reversals to examine the connections of RC cladding panels instead of using a real RC precast structure. The wire mesh reinforcement was used in the panels. The yield strength of the reinforcement was 500 MPa. The compressive strength of concrete was 30 MPa. Threated holes were generated at the edges of RC panels during production.

The SCs were installed in panel-to-beam (PB), panel-to-panel (PP), or panel-to-support (PS) (foundation beam) connections. It was presumed that the SCs used in the PB and PS connections work as mechanical connecters, and the SCs used in the PP connection work as energy dissipaters. The relative vertical displacement between adjacent RC panels is the source of energy dissipation in the PP connection. More than one SC may be used in the PP connection. The designations of the test specimens in terms of the location and thickness of the SCs are listed in Table 1.

Ten tests were done. The properties of further test specimens were decided based on the observations obtained from earlier tests. Table 2 explains the test variables, the goal of the tests, and the test ID numbers.

The experimental study was performed using a specially designed four-hinged steel testing frame, as shown in Fig. 1a and b. Two pairs of cladding panels were mounted at the front and back sides of the testing frame. Hence, two identical panel systems were tested simultaneously. Lateral loading was applied by a servo-controlled hydraulic actuator that was connected to the upper beam of the testing frame. Four steel trusses were used to avoid possible out-of-plane movements of the testing frame. The geometries of the panel systems and SCs placements are shown in Fig. 1c.

It is clear that the SC dimensions affect the force and energy dissipation properties of the device and the embedded system. The determination of the strength and deformation capabilities of SCs was examined in earlier studies in the research group [15–18]. The optimized geometry of SCs was used in the current study to evaluate its effect on the energy dissipation capacity of the RC panel systems. All of them had the same geometry except for their plate thickness (t). The yield strength of the steel used to produce the SCs was determined as 325, 300, and 375 MPa for 3, 5, and 8-mm thick sheets, respectively.

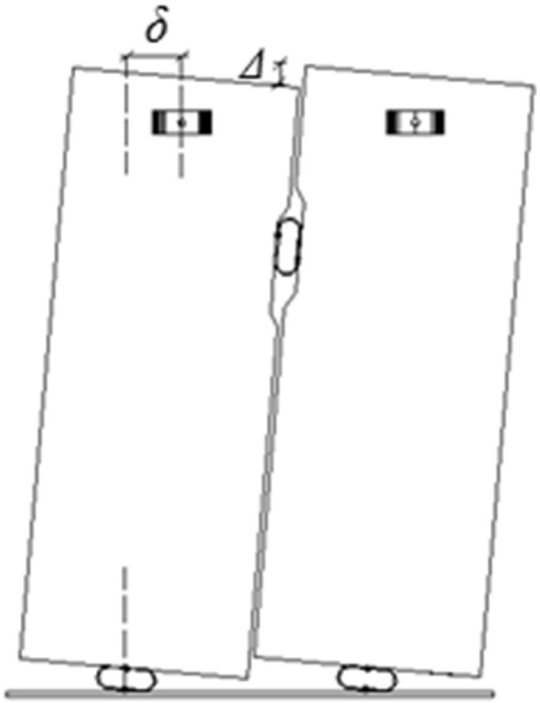

Fig. 3. Definitions of the relative displacements.

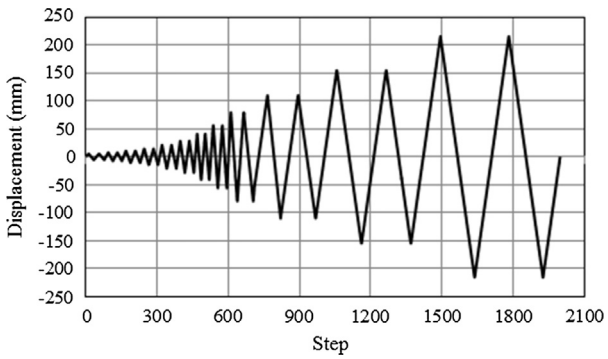

Fig. 4. Displacement protocol used in the experimental study.

Both straight faces of SCs have one hole with a diameter of 30 mm. 8.8 quality M28 bolts were used for the connections of SCs and RC panels, as shown, in Fig. 1c.

2.2. Measurement system and loading protocol

The essential displacements and deformations of the panels were measured by displacement transducers and strain gauges. The pairs of RC panels located at both sides of the loading frame were tagged as "front" (f) and "rear" (r). The locations of the displacement transducers are indicated by TR_f (n) and TR_r (n) in Fig. 2. Several displacement components, including δ and Δ are illustrated in Fig. 3. Precarious deformations of SCs were recorded and compared for the specimens, as shown in Fig. 2d.

The base rotation ϕ_{ij} of the panels is calculated using Eq. (1) through translational displacements of TR(14) – TR(15) and TR(16) – TR(17) for both faces of the test setup. L_{ij} is the distance between the transducers.

$$\phi_{ij} = \frac{TR(i) - TR(j)}{L_{ij}} \quad (1)$$

The displacement protocol used in the tests was selected in accordance with the recommendations of FEMA 461 [19]. The displacement targets were obtained by multiplying ratios a_i/a_{10} by the expected maximum displacement amplitude (δ_m). Two full cycles were applied for each displacement target, as shown in Fig. 4.

3. Experimental results

Fig. 5 presents the actuator force versus the top displacement (δ) hysteresis and their envelopes for the specimens with a single SC at PS connection. S-PB3.PP5.PS8 and S-PB8.PP5.PS8 had strength capacities of 8 kN and 10 kN, respectively. The thickness of the SC located at the beam level had a slight effect on the global strength. S-PB8.PP8.PS8 had a strength of 25 kN, which is much larger than that of S-PB8.PP5.PS8. Hence, a thicker SC in the PP connection has a great effect on the global strength.

Photos were taken at the last cycles of the tests and are presented in Fig. 5. All specimens exhibited large out-of-plane deformations as a common response. The panels moved independently, so the continuity of the cladding surface was disturbed, as shown in Fig. 6.

Fig. 7 presents the force versus top displacement hysteresis and their envelopes obtained for the specimens with double SCs in the PS connection. The ultimate strengths were 30 kN, 4 kN, 10 kN, 20 kN, and 17 kN for the specimens given in Fig. 7. The specimens with the maximum and minimum strengths were D-PB5.PP5.PS8 and D-PB8.PS3, respectively. Consequently, the global lateral strength strongly depends on the presence of the SC in the PP connection.

D-PB8.PP5.PS5 and D-PB8.PP3.PS5 had strengths of 20 kN and 15 kN, respectively. The thicker SC in the PP connection resulted in greater global lateral strength. The out-of-plane deformations observed in the panels were negligible, so the surface continuity of the cladding system was preserved.

No damage was observed in the RC cladding panels. Plastic deformations accumulated on the SCs located at different positions. Hence, the global behavior of the RC cladding system can be adjusted by appropriately selected SCs. Table 3 shows the important test results, including the initial stiffness, ductility ratio, and maximum shear displacement (Δ) between the panels. The elastic displacement ranges are larger in this case.

4. Evaluation of test results

4.1. Panel-to-panel (PP) connection

The performance of the cladding systems was evaluated in terms of the contributions of SCs placed in different types of connections. The effect of the PP connection on the global cyclic behavior of the cladding system was investigated using specimens S-PB8.PP5.PS8, S-PB8.PP8.PS8, D-PB8.PS3, D-PB8.PS3.PP5, D-PB8.PP5.PS, and D-PB8.PP3.PS5.

4.1.1. System tests IV and V (S-PB8.PP5.PS8, S-PB8.PP8.PS8)

5 and 8-mm thick SCs were used in PP connections of S-PB8.PP5.PS8 and S-PB8.PP8.PS8, respectively. Fig. 8a and b present the force versus global displacement (δ) and the relative PP connection displacement (Δ) relations. The restoring forces obtained from tests IV and V were 12 kN and 25 kN, respectively. The plate thickness of the SC used in test IV in the PP connection was thinner than that of the one used in test V, so the restoring force was smaller.

The SCs in the PP connection efficiently increase the lateral strength and stiffness of the cladding system. Fig. 9 shows the ultimate condition of the SCs and their measured strains in the PP connection. The strain gauge measurements show that the SCs in the PP connection yielded.

Test V resulted in greater lateral strength and stiffness, but test IV had a better cyclic response in terms of the deformation shape of the SCs located at the PP connection. The possible reasons are large out-of-plane deformations and the selected plate thickness of SCs at the PP connection. It can be dependently supposed that the plate thickness of

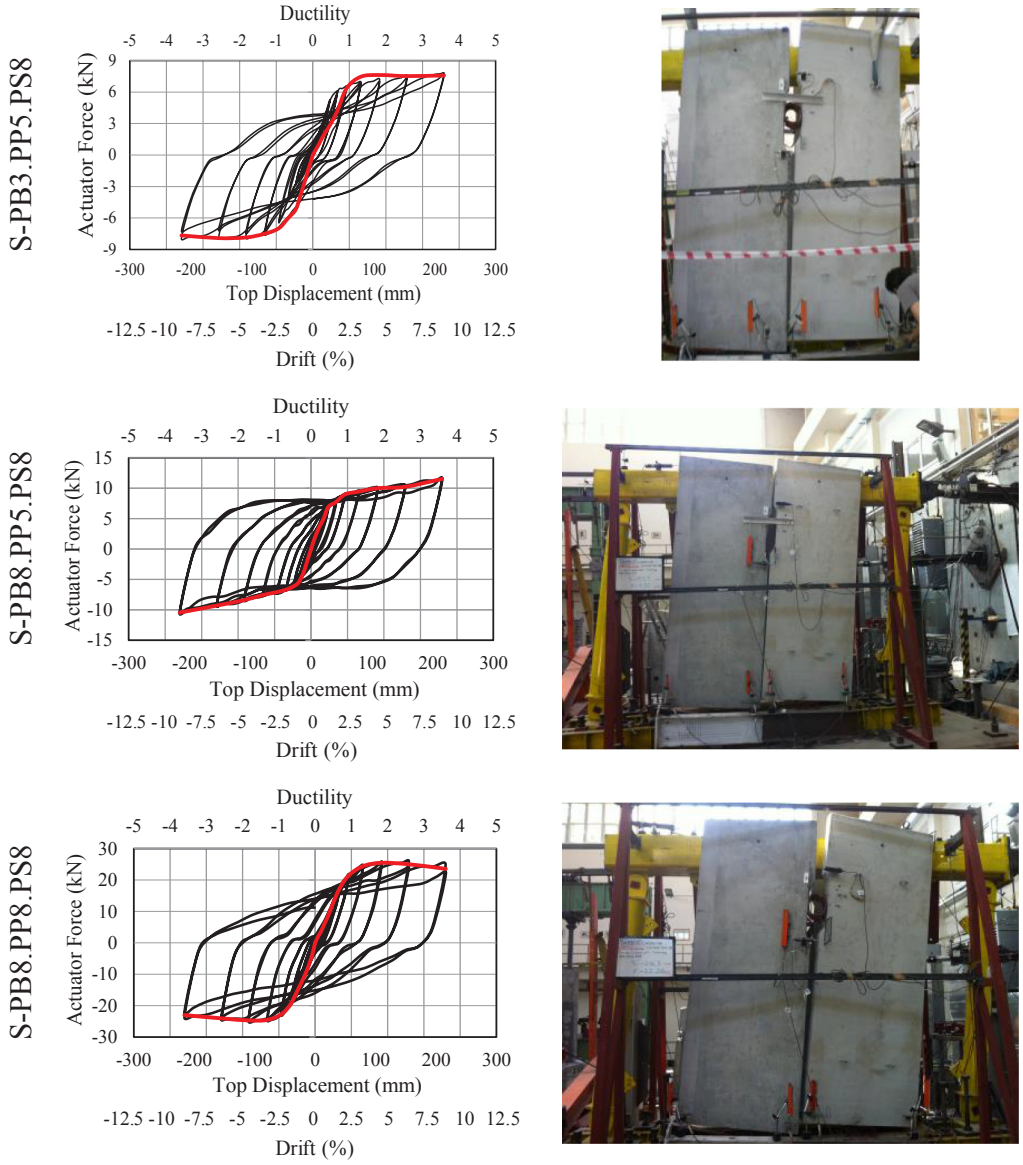

Fig. 5. Force-displacement relations and last-step photos of the specimens with a single SC in the PS connection.

(a) Large out of plane deformations of panels (b) Large deformation of *SC* at *PP connection*

Fig. 6. Common damage of the specimens with a single SC in the PS connection.

out of plane SC used in the PP connection should be thinner than the others. Fig. 10 shows the cumulative energy dissipation, equivalent damping, and secant stiffness in terms of the drift ratio.

The cumulative energy dissipation and secant stiffness were greater in test V than test IV. As the SC at the PP connection becomes thicker, the relative vertical displacement between adjacent panels becomes smaller. Consequently, the lateral strength and stiffness of the system become greater. However, better equivalent damping was obtained for test IV.

4.1.2. System tests VI and VII (D-PB8.PS3, D-PB8.PP5.PS3)

Both specimens D-PB8.PS3 and D-PB8.PP5.PS3 had two SCs at the bottom. However, there was an SC in the PP connection in test VII. Fig. 11a and 11b show the global force-displacement (δ) relations of the specimens and force-displacement (Δ) relation obtained at the PP connection in test VII.

The ultimate restoring forces derived from tests VI and VII were 4.5 kN and 10 kN, respectively. The relative displacement of the SC in the PP connection in test VII was about 60 mm. It was clear that the foremost reason for the difference between the restoring forces was the presence of the SC in the PP connection. The strength contribution of the 5-mm thick SC in the PP connection to the global response was almost 50%. Photographs were taken of the PP connection in tests VI and VII and are shown in Fig. 12. The strain measurement on the SC in the PP connection is shown in Fig. 12. It is shown that the SC reached

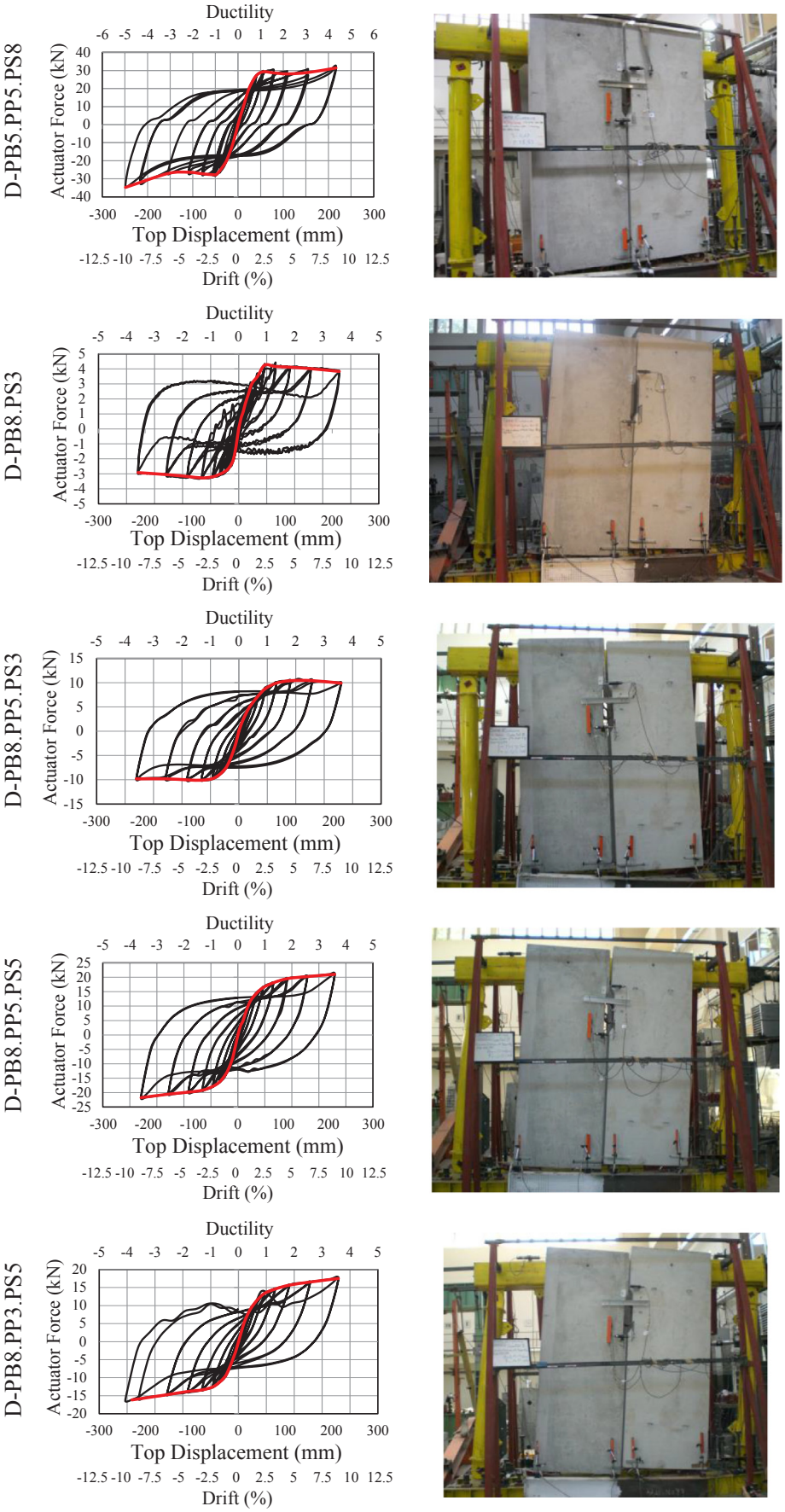

Fig. 7. Force-displacement relations and last-step photos of the specimens with double SCs in the PS connection.

Table 3
Summary of the test results.

Specimen	Stiffness (kN/mm)	Yielding disp. (mm)	Ultimate force (kN)	Ultimate disp. (mm)	Ductility ratio	Max. vert. disp. between panels (mm)
S-PB3.PP5.PS8	0.120	55.7	7.66	215.5	3.9	31.8
DPB3.PP5.PS8	0.447	20.9	14.52	215.4	10.3	4.3
D-PB5.PP5.PS8	0.556	51.1	34.78	248.8	5.4	23.8
S-PB8.PP5.PS8	0.144	55.7	11.53	216.1	3.9	87.7
S-PB8.PP8.PS8	0.396	55.8	25.49	216.3	3.9	62.3
D-PB8.PS3	0.067	55.9	4.25	215.4	3.9	N.A.
D-PB8.PP5.PS3	0.166	55.8	10.42	216.1	3.9	77.8
D-PB8.PP8.PS3	0.231	78.9	21.75	215.2	2.7	64.2
D-PB8.PP5.PS5	0.307	55.8	21.75	215.2	3.9	80.5
D-PB8.PP3.PS5	0.233	55.8	17.51	229.6	4.1	84.4

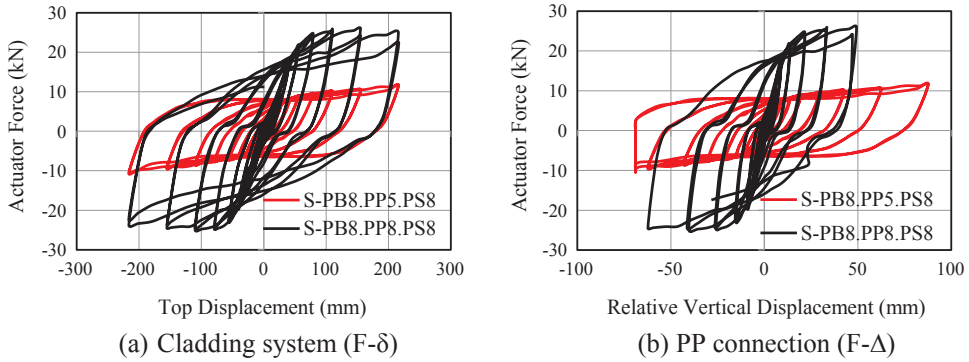

Fig. 8. Force-displacement relations of tests IV and V.

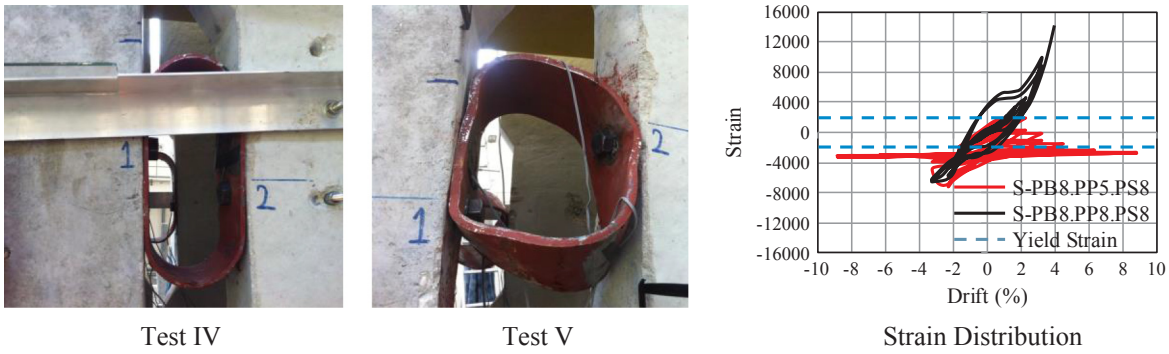

Fig. 9. Ultimate SC deformations in the PP connection of tests IV and V.

the inelastic range. The shear behavior of the SC also had a significant contribution to the global energy dissipation capacity of the system.

Fig. 13a and b show the energy dissipation capacity and equivalent damping ratio variations in terms of the drift from tests VI and VII. The energy dissipation capability and damping ratio of test VII are larger than in test VI. Fig. 13c presents the lateral stiffness versus the drift relation rom tests VI and VII. Test VII had higher stiffness than test VI. The SC in the PP connection increased not only the lateral strength but also the lateral stiffness of the system.

4.1.3. System tests VII and X (D-PB8.PP5.PS3 and D-PB8.PP3.PS5)

Tests VII and X were done to assess the effects of the SCs used in PS and PP connections. Fig. 14a and b show the relations of the global force and displacement (δ) and of the force and displacement (Δ) in the PP connection. Both of the tests resulted in stable force-displacement hysteresis. The ultimate restoring forces obtained from tests X and VII were 15 kN and 10 kN, respectively. However, the plate thickness of the SC used in the PP connection in test VII was bigger than that in test X, which showed higher strength. The reason was that the specimens in test X were supported by thicker SCs. It can be concluded that the SCs used in the support had a more notable effect on the global response than the SC placed in the PP connection.

The ultimate states of the PP connection and the SC strain distributions are shown in Fig. 15. Large strains were obtained in test X. The energy dissipation capability, equivalent damping and, lateral stiffness variations of tests VII and X are shown in Fig. 16a–c. The energy dissipated in test X was greater than that in test VII. The maximum equivalent damping ratios were 40% and 25% for tests VII and X, respectively. The lateral stiffness of test X was higher than in test VII due to the thicker SCs used in the support.

4.2. Panel-to-support (PS) connection

4.2.1. System tests I and II (S-PB3.PP5.PS8 and D-PB3.PP5.PS8)

The effect of the PS connection on the overall cyclic behavior of the cladding system was investigated through comparisons of the results of the specimens D-PB8.PP5.PS3 vs. D-PB8.PP5.PS5 and S-PB3.PP5.PS8 vs. D-PB3.PP5.PS8. The difference between test I and test II is the number of SCs used in the support region. Fig. 17a and b show the force versus displacement (δ) and the force versus the support rotation. In

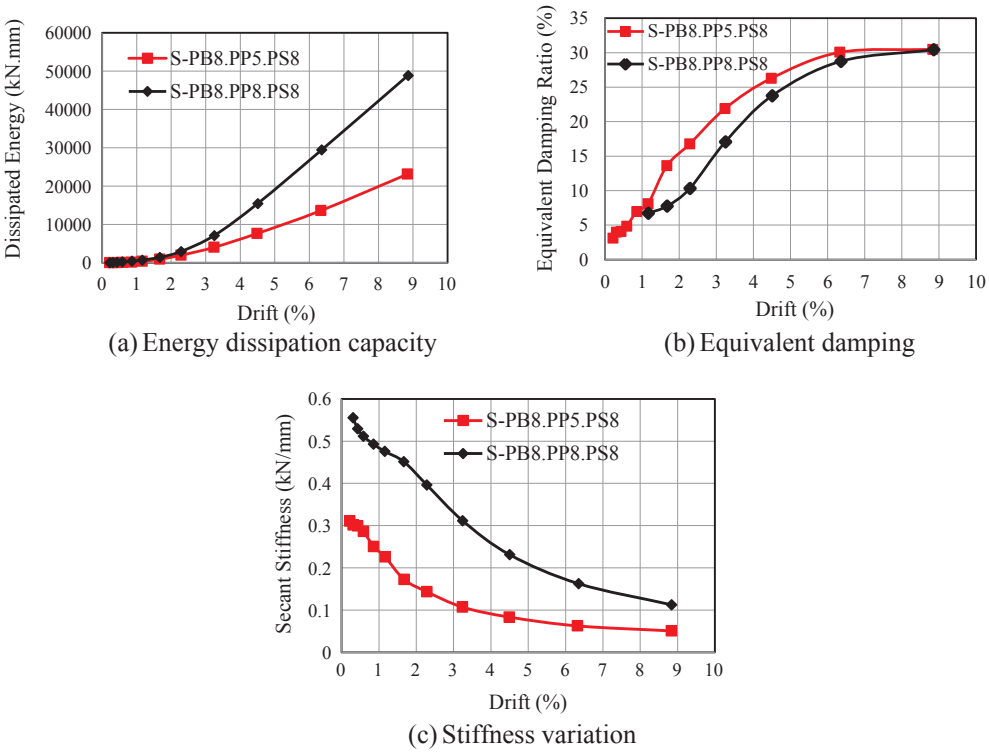

Fig. 10. Evaluation of the results of tests IV and V.

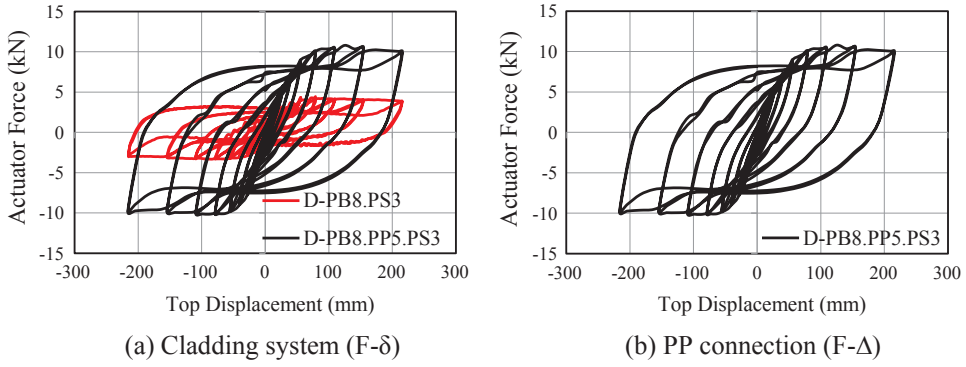

Fig. 11. Force-displacement relations of tests VI and VII.

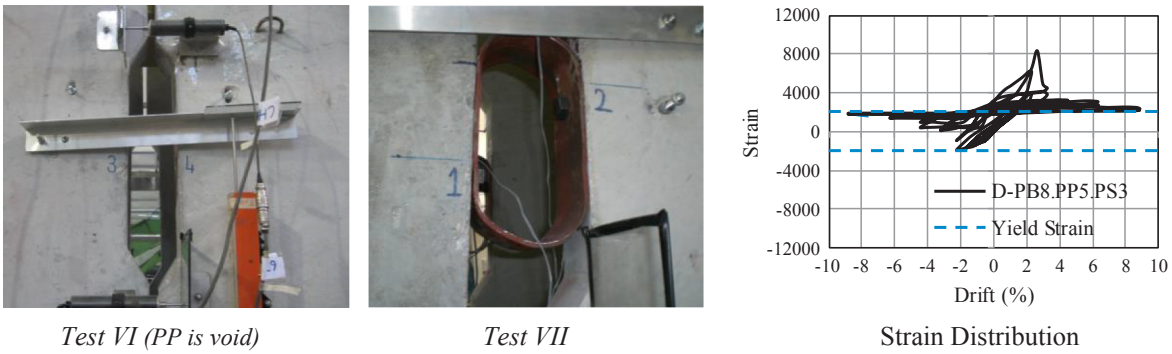

Fig. 12. Ultimate SC deformations in the PP connection of tests VI and VII.

test II, which had two SCs in the support region, higher lateral strength and stiffness were obtained than in test I. The support rotations of test II were particularly lower than in test I. The rotation of cladding panels was restricted by using double SCs in the PS connection.

Photos of the PS connections are presented in Fig. 18. Using double SCs in the support restricts the rotation of the claddings about its lateral and vertical axes. The out-of-plane deformations are presented in Fig. 19. They increased gradually in one direction in both of the tests. The SC with a 3-mm plate thickness used in the PB connection affected the out-of-plane deformation of the cladding system.

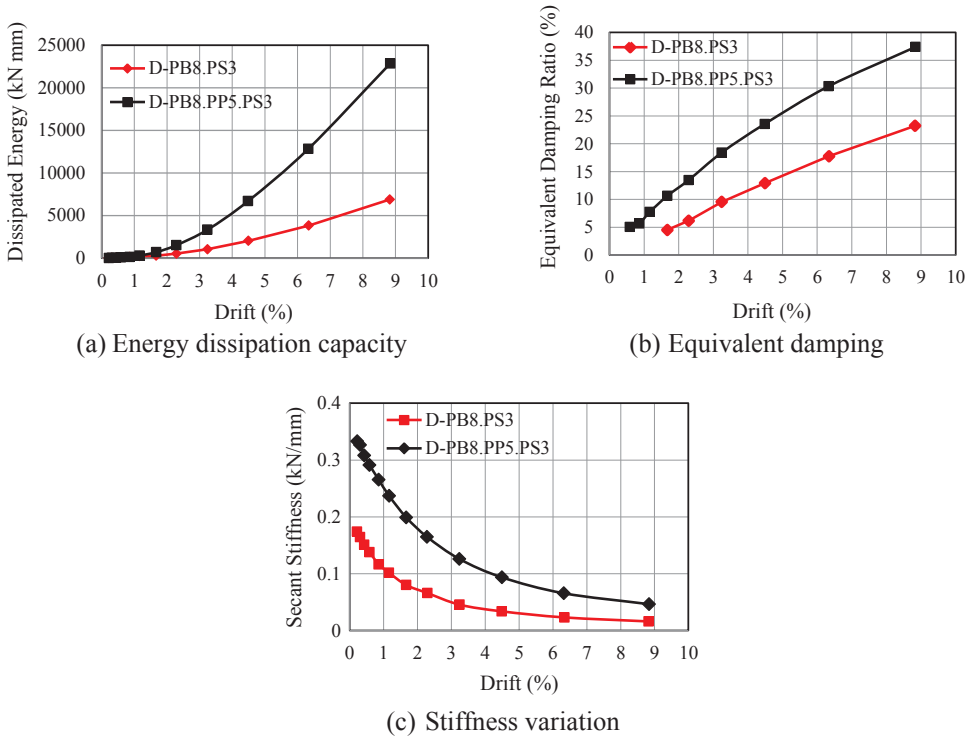

Fig. 13. Evaluation of the results of tests VI and VII.

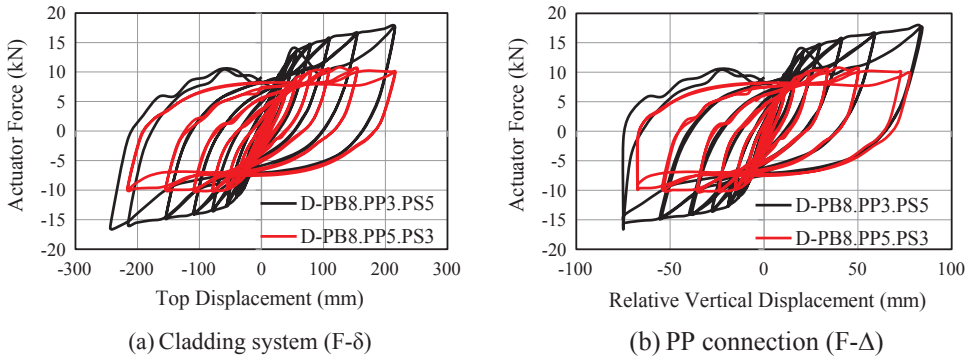

Fig. 14. Force-displacement relations of tests VII and X.

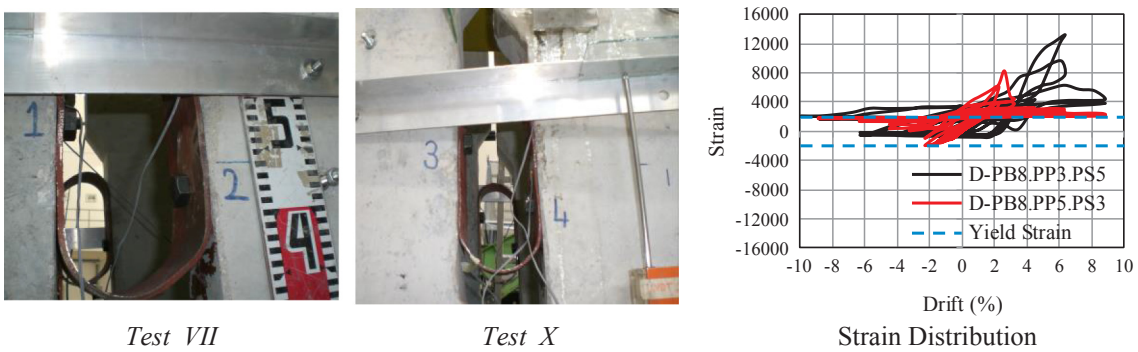

Fig. 15. Ultimate SC deformations in the PP connection of tests VII and X.

Fig. 20 shows the cumulative energy dissipation capability, equivalent damping, and stiffness variations according to the drifts. The energy dissipation capability, equivalent damping, and lateral stiffness properties obtained from test II were better than in test I. The lateral stiffness of test II was greater than in test I up until a drift of 3%. After this point, the lateral stiffness of both specimens became similar, as shown in Fig. 20c.

4.2.2. System tests VII and IX (D-PB8.PP5.PS3 and D-PB8.PP5.PS5)

The plate thicknesses of the SCs used in the PS connection were

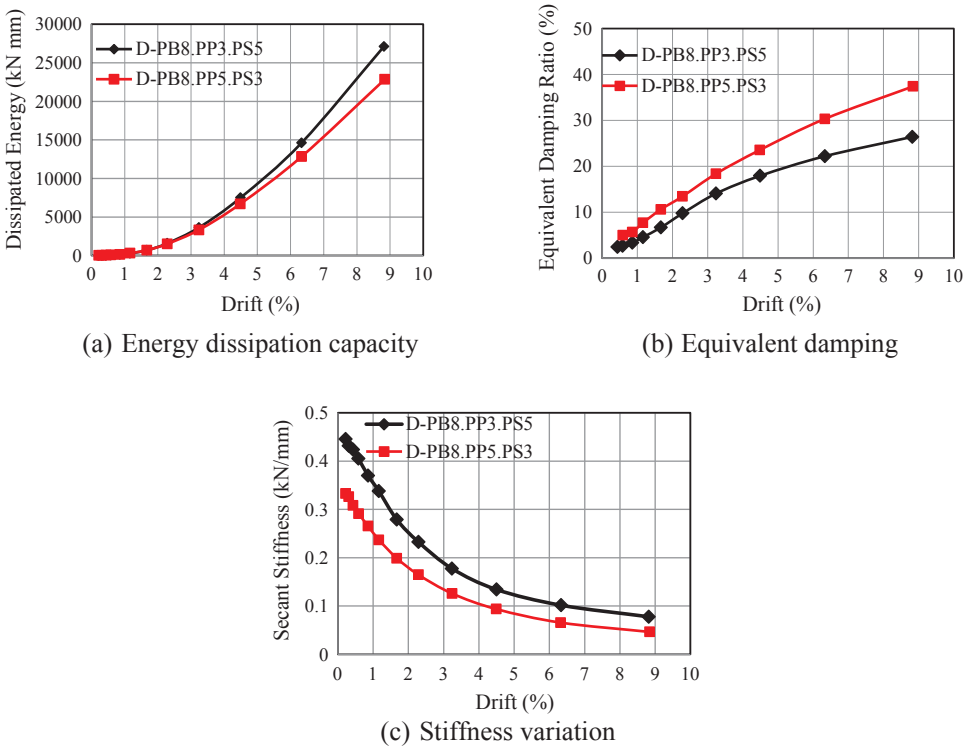

Fig. 16. Evaluation of the results of tests VII and X.

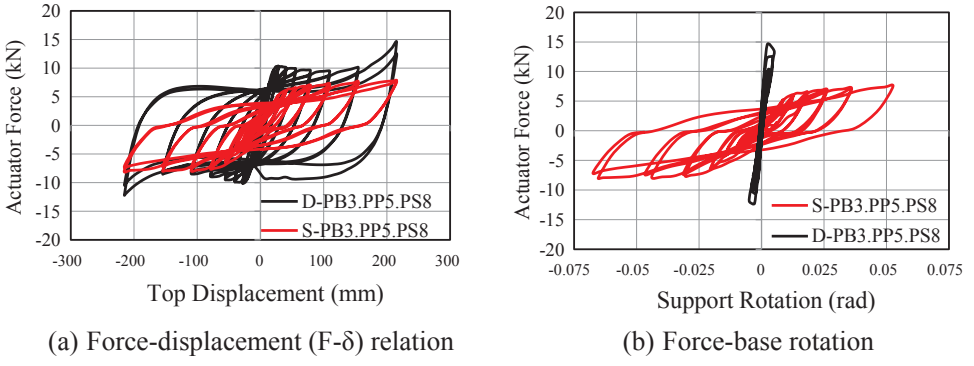

Fig. 17. Force-displacement and force-base rotation relations of tests I and II.

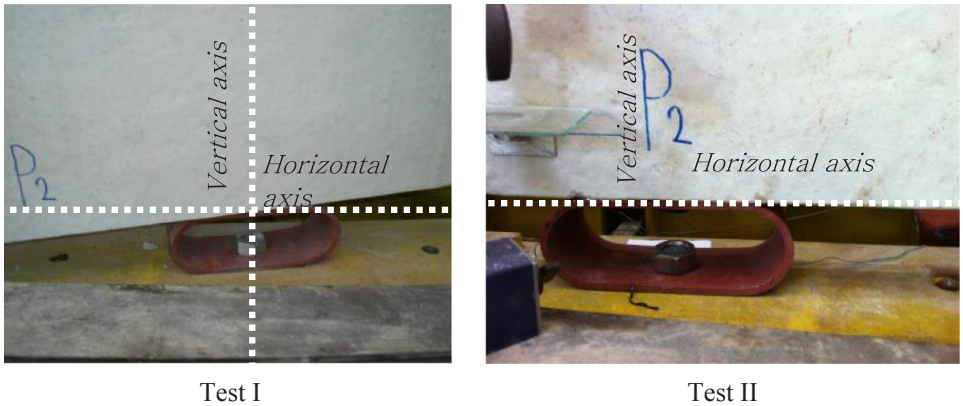

Fig. 18. Base rotation.

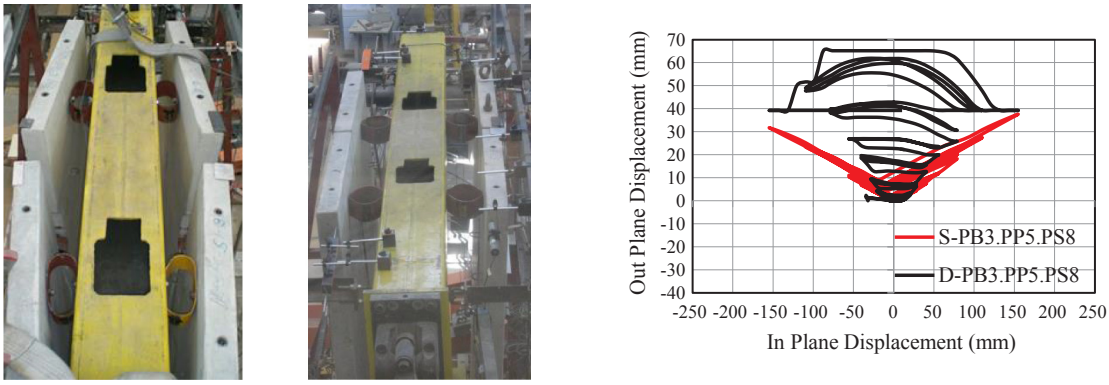

Fig. 19. Out of plane deformations.

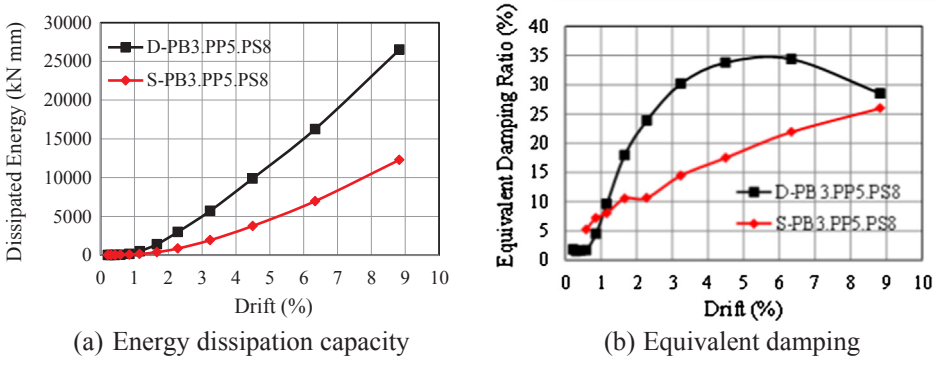

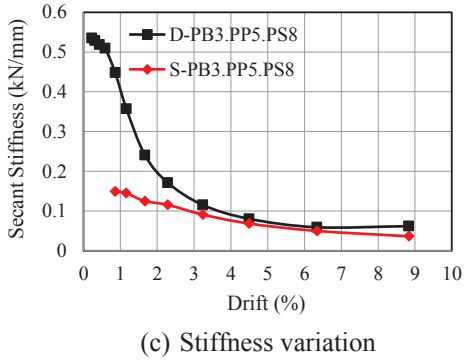

Fig. 20. Evaluation of the results of tests I and II.

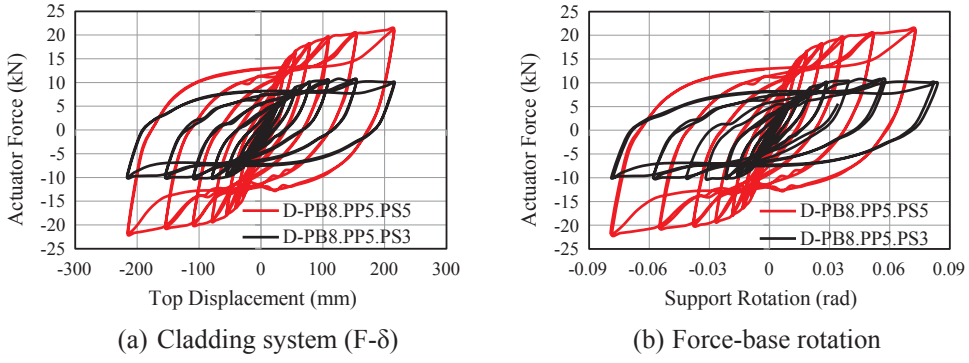

Fig. 21. Force-displacement and force-base rotation relations of tests VII and IX.

Fig. 22. Photos from PS connections and strain distribution on SCs.

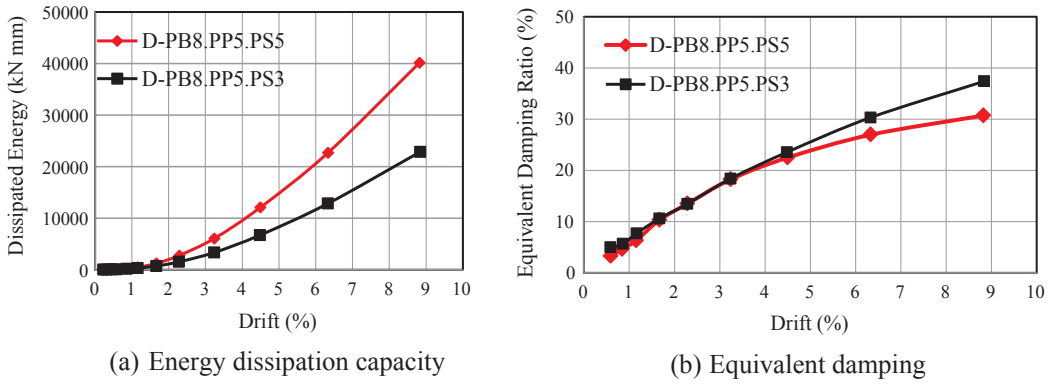

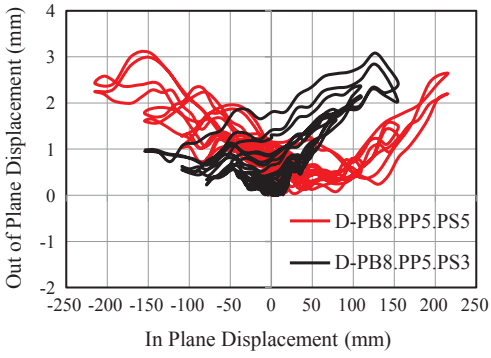

Fig. 23. Evaluation of the results of tests VII and IX.

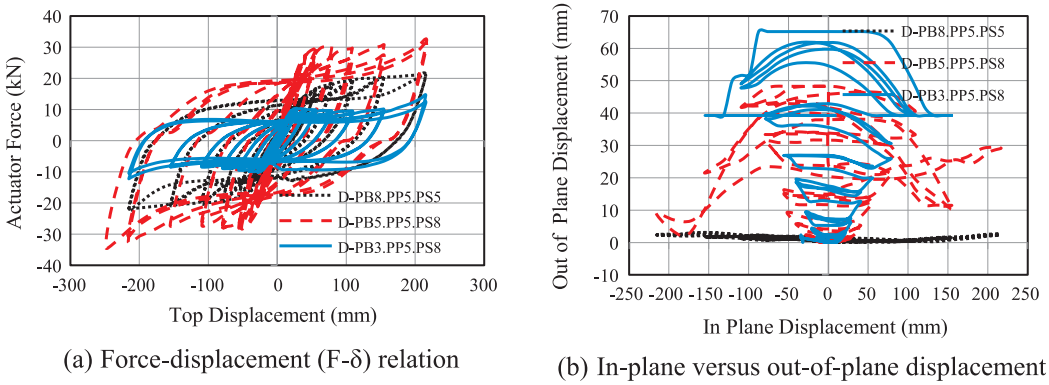

Fig. 24. Force-displacement relations of tests II, III, IX.

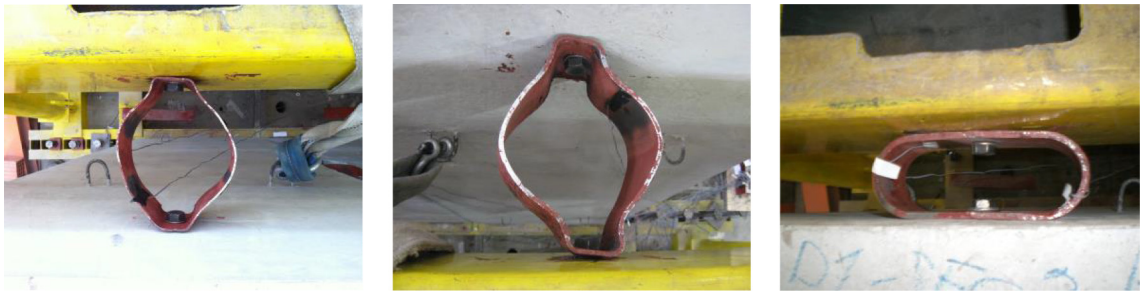

Fig. 25. Deformed shapes of SCs in the PB connection (top view).

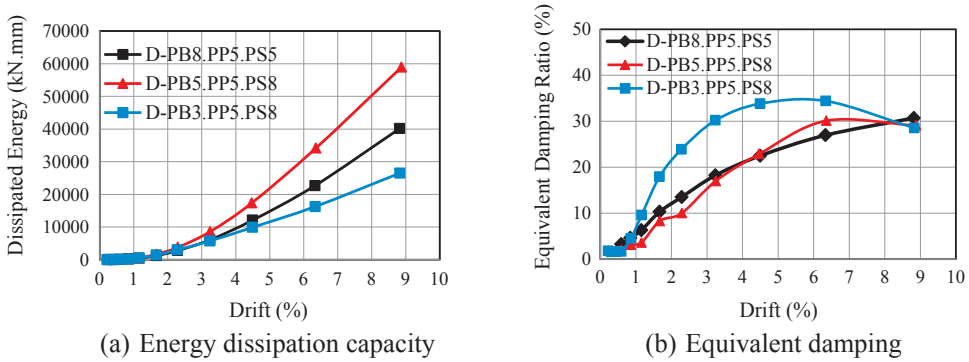

Fig. 26. Evaluation of the results of tests II, III, and IX.

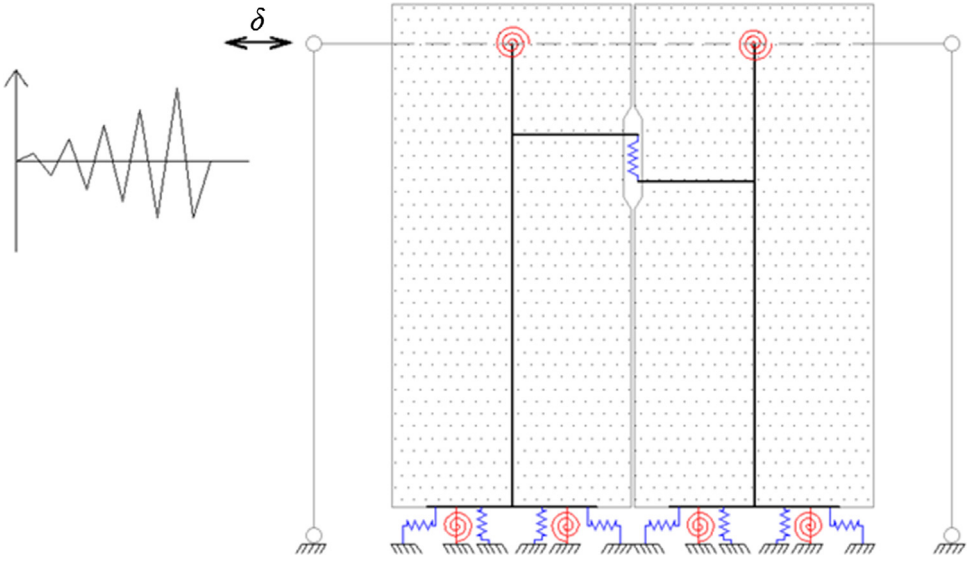

Fig. 27. Numerical model for the tested specimens.

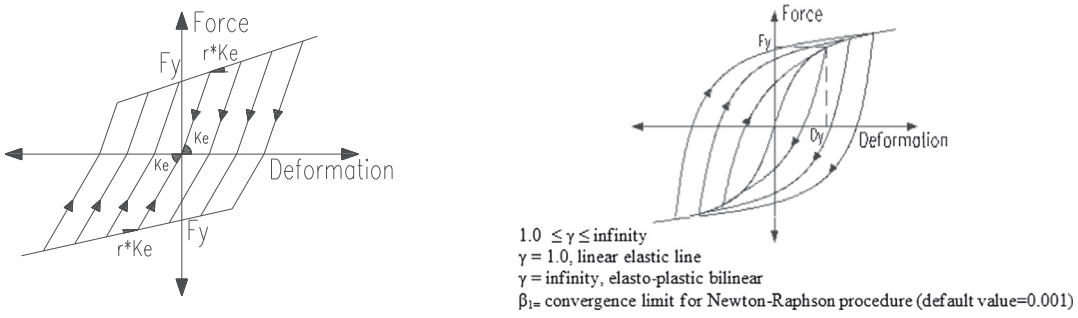

(a) Asymmetric bi-linear model used for SCs in the PS connection

(b) Ramberg-Osgood Model [21] used for SCs in the PP connections

Fig. 28. Cyclic behavior models used in the analyses.

Table 4
Numerical model parameters for test VII (D-PB8.PP5.PS3).

Location	Connection	Action	Properties of the link elements		
PP	5-mm-thick SC	Shear	Ramberg Osgood [21]		
			F_y = 7.8 kN	D_y = 10.92 mm	$\gamma = 20\ \beta_1 = 0.001$
		Normal	Linear Elastic		
			k_0 = relatively high stiffness		
PS	3-mm-thick SC	Shear	Ramberg Osgood		
			F_y = 2.5 kN	D_y = 13.50 mm	$\gamma = 20\ \beta_1 = 0.001$
		Normal (comp.)	Bi-Linear Asymmetric		
			F_y = 6.0 kN	K_e = 0.57 kN/mm	r = 0.1
		Normal (tension)	Ramberg Osgood		
			F_y = 2.5 kN	D_y = 13.54 mm	$\gamma = 10\ \beta_1 = 0.001$
		Bending	Linear Elastic		
			k_0 = relatively low stiffness		
PB	8-mm-thick SC	Shear	Ramberg Osgood		
			F_y = 27.8 kN	D_y = 10.91 mm	$\gamma = 20\ \beta_1 = 0.001$
		Bending	Linear Elastic		
			k_0 = relatively low stiffness		
		Normal	Linear Elastic		
			k_0 = relatively low stiffness		

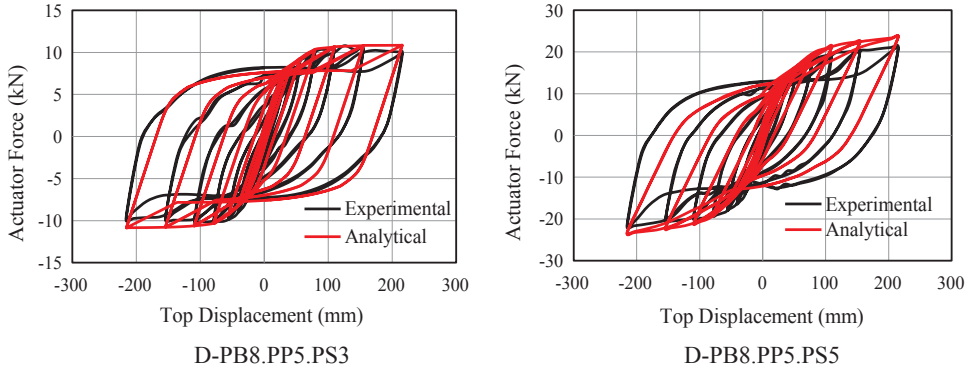

Fig. 29. Numerical versus experimental restoring force-lateral displacement (δ) relations.

different between the specimens. Fig. 21a and b show the restoring force versus elative lateral displacement (δ) and the force versus the base rotation. The ultimate lateral strengths obtained from tests IX and VII were 20 kN and 10 kN, respectively. The maximum relative displacements (Δ) of the SCs in the PP connection were 77.78 and 78.60 mm for tests VII and IX. The maximum base rotations of the claddings were 0.079 and 0.075 rad, respectively. The increment of the plate thickness of the SCs in the PS connection improves clearly the general behavior of the cladding system.

Photos of the PS connections and strain versus the drift relations on the SC are presented in Fig. 22. SCs in the PS connection yielded in the tests. The SCs with thicknesses of 3 or 5 mm in the support may dissipate a considerable amount of energy.

Fig. 23a and b show the variations of the energy dissipation capability and equivalent damping in terms of the drift angle for tests VII and IX. The ultimate energy dissipation capacities obtained from tests VII and IX were 22,846 kNmm and 40,131 kN mm, respectively. The 5-mm-thick SCs in the PS connection resulted in a 76% increase in the energy dissipation capacity compared to the results obtained with a 3-mm thickness. The maximum equivalent damping ratios were 37% and

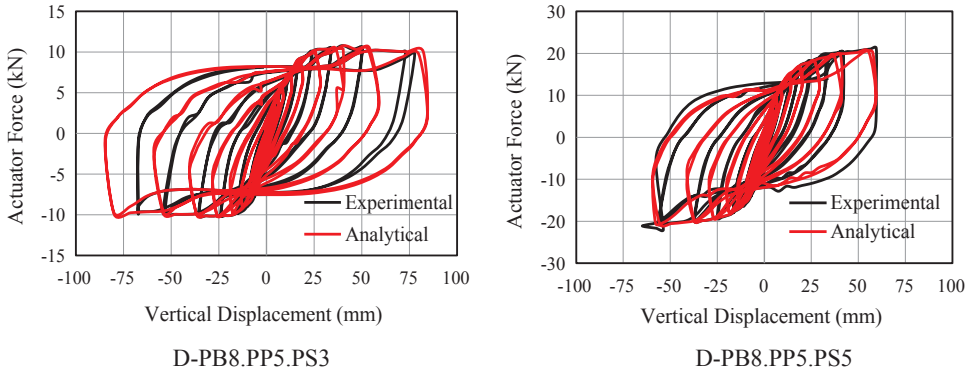

Fig. 30. Numerical versus experimental restoring force-relative panel displacement (Δ) relations.

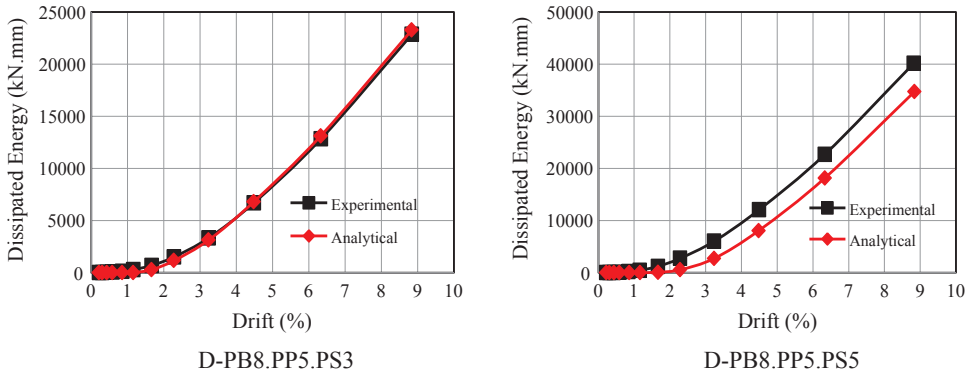

Fig. 31. Comparison of the numerical and experimental cumulative energy diagrams.

31% for tests VII and IX, respectively. Somehow, a reverse relation was obtained between the energy dissipation capacity and equivalent damping ratio.

Fig. 23c shows the in-plane versus out-of-plane displacement variations for tests VII and IX. The out-of-plane displacements were smaller for both tests. The potential reasons are the use of double SCs in the PS connections and the thicker SCs in the PB connections.

The dissipated energy could be increased if the plate thickness of the SC in the PS connection is correctly selected to enable rotation of the cladding panel. On the other hand, the rotation capacity of the panels is also affected by the plate thickness of the SCs located in the PP connection. To obtain more efficient dissipative systems, the SCs located in the PP and PS connections should be selected coherently.

4.3. Panel-to-Beam (PB) connection

The effect of the PB connection on the global behavior of the cladding system was investigated by comparing the results of tests II, III, and IX (D-PB3.PP5.PS8, D-PB5.PP5.PS8, and D-PB8.PP5.PS5). The plate thicknesses of the SCs used in the PB connections for these tests were 3, 5, and 8 mm, respectively. Fig. 24a and b show the force versus displacement (δ) and in-plane versus out-of-plane displacement diagrams. The ultimate restoring forces obtained from tests II, III, and IX were 10 kN, 20 kN, and 30 kN, respectively. The lateral strength of the cladding system increases when the plate thickness of the SCs used in the PP connection is increased.

The maximum out-of-plane displacements recorded in tests II, III, and IX were 70 mm, 50 mm, and 1 mm, respectively. D-PB8.PP5.PS5 (test IX), which had 8-mm-thick SCs in the PB connection, had the smallest out-of-plane displacement. The plate thickness of the SCs in the PB connection affects the out-of-plane deformations. The deformed shapes of the SCs used in the PB connections are shown in Fig. 25.

Fig. 26 shows the cumulative energy dissipation capability, equivalent damping, and stiffness variations. The energy dissipation capacities of the specimens were similar at drift level of up to 2%, but after that, test III had superior energy dissipation capacity. Excessive deformations were observed in the SCs in the PB connection in test II, which also had the maximum equivalent damping. The stiffness variations were in the same order as the energy dissipation capacities. The lateral stiffness obtained from test III was higher than in test II, where the difference between the specimens was the plate thickness of the SCs in the PB connections.

5. Numerical studies

5.1. Modeling strategy

The experimental results of D-PB8.PP5.PS3 and D-PB8.PP5.PS5 were reproduced numerically by means of models generated in Seismostruct [20]. The structural model consists of the pinned steel frame and the cladding system. The representative structural model is illustrated in Fig. 27. The members of the pinned steel frame were modeled by linear-elastic frame elements with flexural hinges at both ends. The RC cladding panels were modeled by linear elastic frame elements defined at the center of the panels. Infinitely rigid arms were used to fix various SCs. Depending on the experimental observations, nonlinear link elements were used to model the response of the SCs located in different locations. The cyclic behavior models used in the analyses are shown in Fig. 28.

The parameters of the nonlinear link elements used for test VII (D-PB8.PP5.PS3) are listed in Table 4. The yield force, yielding displacement, and ultimate displacement of the SC were determined according to the geometric and material properties by using previously derived equations [15,16].

5.2. Numerical results

Nonlinear static time history analyses were performed using SeismoStruct for the displacement protocol used in the experiment, as shown in Fig. 3. The obtained restoring force versus lateral displacement (δ) and the restoring force versus relative panel displacement (Δ) for D-PB8.PP5.PS3 and D-PB8.PP5.PS5 were compared with the corresponding experimental results, as shown in Figs. 29 and 30.

The numerical model is capable of predicting the maximum strength and displacement capacities. Moreover, the model satisfactorily captures the loading and unloading branches of the force-displacement relations. The cumulative dissipated energy diagrams derived from the experimental and numerical studies are given in Fig. 31. The numerical and experimental cumulative energy diagrams are consistent with each other.

6. Conclusions

The usage of steel cushions in the connections of RC cladding panels was studied experimentally. The following conclusions were obtained:

1. No damage was observed on the RC cladding panels, and they remained in the elastic range. Plastic deformations accumulated on the SCs. They may be replaced after having large plastic deformation.
2. The shear deformation of the SCs in the PP connection and the combined normal and shear deformations of the SCs in the PS connection had greater contributions to the global energy dissipation capacity than the one in the PB connection.
3. The plate thickness of the SCs in the PP connections should be thinner than the others to obtain robust energy dissipation capability. Otherwise, the cladding system may act either as an integrated shear wall system or a system with undesirable out-of-plane deformation.
4. Displacement ductility ratios reached in the RC cladding systems were around 5.
5. The specimens with double SCs in the PS connection has stable cyclic behavior till structural drift ratio of 8%.
6. The out-of-plane deformations of the cladding panels may be decreased by using double SCs in the PS connection as well as a thicker SC in the PB connection.
7. Ramberg-Osgood and asymmetric bi-linear behavior models were effective to predict the behaviors of the SCs. The global cyclic behavior of the cladding system was well predicted.
8. Higher structural damping was achieved by appropriately selecting the thickness and locations of the SCs in the RC cladding system.
9. The SC does not have a re-centering capability. The residual displacements of the RC panel system should be restricted to maintain the continuity in the façades of the building by arranging the geometry of the SCs.

Acknowledgements

This research was conducted in the framework of the FP7 project, “SAFECLADDING: Improved Fastening Systems of Cladding Wall Panels of Precast Buildings in Seismic Zones,” research for SME associations, grant agreement number 314122, which was coordinated by Mr. Alessio Rimoldi from BIBM. The financial support provided by the Commission of the European Communities through this project is greatly appreciated. The study was conducted at the Structural and Earthquake Engineering Laboratory (STEELab) of Istanbul Technical University. The support of the laboratory staff and graduate students is gratefully acknowledged.

Appendix A. Supplementary material

Supplementary data to this article can be found online at https://doi.org/10.1016/j.engstruct.2019.03.092.

References

[1] Ercolino M, Maglilulo G, Manfredi G. Seismic performance of single-story precast buildings: effect of cladding panels. J Stuct Eng 2018;144(9):04018134.
[2] Priestley MJN, Sritharan S (Sri), Conley JR, Stefano Pampanin S. Preliminary results and conclusions from the PRESSS five-story precast concrete test-building. PCI J 1999;44:42–67.
[3] Psycharis IN, Kalyviotis I, Mouzakis HP. Experimental and numerical investigation of the fixed connections of RC cladding walls to precast building. Second Eur Conf Earthq Eng Seismol, Istanbul, Turkey; 2014.
[4] Biondini F, Dal Lago B, Toniolo G. Role of wall panel connections on the seismic performance of precast structures. Bull Earthq Eng 2013;11:1061–81.
[5] Dal Lago B, Biondini F, Toniolo G. Seismic performance of precast concrete structures with energy dissipating cladding panel connection systems. Struct Concr 2018:1–19.
[6] Dal Lago B, Tornaghi M Lamperti. Sliding channel cladding connections for precast structures subjected to earthquake action. Bull Earthq Eng 2018;16:5621–46.
[7] Dal Lago B, Biondini F, Toniolo G. Friction-based dissipative devices for precast concrete panels. Eng Struct 2017;147:356–71.
[8] Del Monte E, Falsini C, Boschi S, Menichini G, Orlando M. An innovative cladding panel connection for RC precast buildings. Bull Earthq Eng 2019;17:845–65.
[9] Dal Lago B, Bianchi S, Biondini F. Diaphragm effectiveness of precast concrete structures with cladding panels under seismic action. Bull Earthq Eng 2019;17(1):473–95.
[10] Kelly JM, Skinner RI, Heine AJ. Mechanisms of energy absorption in special devices for use in earthquake resistant structures. Bull New Zeal Soc Earthq Eng 1972;5:63–88.
[11] Oh SH, Kim YJ, Ryu HS. Seismic performance of steel structures with slit dampers. Eng Struct 2009;31:1997–2008.
[12] Schultz AE, Magana RA. Seismic behavior of connections in precast concrete walls. Mete A. Sozen Symposium, Am Concr Inst, Farmington Hills, MI, USA; 1996.
[13] Chan RWK, Albermani F. Experimental study of steel slit damper for passive energy dissipation. Eng Struct 2008;30:1058–66.
[14] Biondini F, Dal Lago B, Toniolo G. Experimental and numerical assessment of dissipative connections for precast structures with cladding panels. Second Eur Conf Earthq Eng Seismol, Istanbul, Turkey; 2014.
[15] Yüksel E, Karadoğan F, Özkaynak H, Khajehdehi A, Güllü A, Smyrou E, et al. Behaviour of steel cushions subjected to combined actions. Bull Earthq Eng 2018;16:707–29.
[16] Özkaynak H, Khajehdehi A, Güllü A, Azizisales F, Yüksel E, Karadoğan F. Uni-axial behavior of energy dissipative steel cushions. Steel Compos Struct 2018;27:661–74.
[17] Özkaynak H, Güllü A, Gökçe T, Khajehdehi A, Mahdavi MA, Azizisales F, et al. Energy dissipater steel cushions. Second Eur Conf Earthq Eng Seismol, Istanbul, Turkey; 2014.
[18] Özkaynak H, Güllü A, Khajehdehi A, Gökçe T, Azizisales F, Bal İE, et al. Bi-directional loading tests of steel cushions. 14th World Conf Seism Isol Energy Dissipation Act Vib Control Struct, San Diego, Ca USA; 2015.
[19] FEMA461. Interim testing protocols for determining the seismic performance characteristics of structural and nonstructural components. Federal Emergency Management Agency (FEMA), Washington (DC), USA; 2007.
[20] Seismostruct v7.0. A computer program for static and dynamic nonlinear analysis of framed structures. Available from < http://www.seismosoft.com > .
[21] Ramberg W, Osgood WR. Description of stress-strain curves by three parameters. Washington (DC), USA: National Advisory Committee for Aeronautics; 1943.